The Cryosphere Discuss., doi:10.5194/tc-2016-262, 2016
Manuscript under review for journal The Cryosphere
Published: 19 December 2016

The Cryosphere Discussions
Open Access
EGU

Evaluation of snow cover and snow depth on the Qinghai-Tibetan Plateau derived from passive microwave remote sensing

Liyun Dai[1], Tao Che [1,2], Yongjian Ding [3], Xiaohua Hao [1]
[1]Key Laboratory of Remote Sensing of Gansu Province, Heihe Remote Sensing Experimental Research Station, Cold and Arid Regions Environmental and Engineering Research Institute, Chinese Academy of Sciences, Lanzhou 730000, China
[2]Center for Excellence in Tibetan Plateau Earth Sciences, Chinese Academy of Sciences, Beijing 100101, China
[3] State Key Laboratory of Cryospheric Sciences, Cold and Arid Regions Environmental and Engineering Research Institute, Chinese Academy of Sciences, Lanzhou 730000, China

Correspondence to: Tao Che (chetao@lzb.ac.cn)

Abstract. Snow cover on the Qinghai-Tibetan plateau (QTP) plays a significant role in the global climate system and is an important water resource for rivers in the high elevation region of Asia. At present, passive microwave (PM) remote sensing data are the only efficient way to monitor temporal and spatial variations in snow depth at large scale. However, existing snow depth products show the largest uncertainties across the QTP. In this study, MODIS fractional snow cover product, in situ observations, and airborne observation data are synthesized to evaluate the accuracy of snow cover and snow depth derived from PM remote sensing data and to analyze the possible causes of uncertainties. The results show that the accuracy of snow cover extents varies spatially and depends on the fraction of snow cover. Based on the assumption that grids with MODIS snow cover fraction > 10 % are regarded as snow cover, the overall accuracy in snow cover is 66.7 %, overestimation error is 56.1 %, underestimation error is 21.1 %, commission error is 27.6 % and omission error is 47.4 %. The commission and overestimation errors of snow cover primarily occur in the northwest and southeast areas with low ground temperature. Omission error primarily occurs in cold desert areas with shallow snow, and underestimation error mainly occurs in glacier and lake areas. Comparison between snow depths measured in field experiments, measured at meteorological stations and estimated across the QTP shows that agreement between observation and retrieval improves with an increasing number of observation points in a PM grid. The misclassification and errors between observed and retrieved snow depth are associated with the relatively coarse resolution of PM remote sensing, ground temperature, snow characteristics and topography. To accurately understand the variation in snow depth across the QTP, new algorithms should be developed to retrieve snow depth with higher spatial resolution and should consider the variation in brightness temperatures at different frequencies emitted from ground with changing ground features.

1 Introduction

The Qinghai-Tibetan plateau (QTP) is considered the third pole of the world; its snow cover is an indicator of global climate change (Kang et al., 2010; Wu et al., 2003; Wang et al., 2015), and snow cover variation impacts the near ground air

The Cryosphere Discuss., doi:10.5194/tc-2016-262, 2016
Manuscript under review for journal The Cryosphere
Published: 19 December 2016

temperature and precipitation in Eurasia and across the Northern Hemisphere (Zhang et al, 2004; Lü et al., 2008; You et al., 2011). It is also regarded as the Asian water tower, contributing a large portion of the water supply of China (Immerzeel et al., 2010; Xu et al., 2008). Due to its importance regionally and globally and evident change (Shi and Wang, 2015), more attention should be paid to the snow cover variability across the QTP. Monitoring snow cover variability requires reliable snow depth and snow cover data.

Traditional station observation is used to monitor inter-annual variation of snow depth at local or regional scales. Inter-annual changes in snow cover and depth in Russia was analyzed using snow depths observed at 856 stations (Bulygina et al., 2009). Zhong et al. (2014) used station observation to analyze the snow density of Eurasian region. It was also use to longer the time series analysis due to its long history (Gafurov et al., 2015). However, meteorological station data do not always represent the snow status of a region, especially in regions with few stations, such as the QTP, although there are some studies that have reported spatiotemporal variation across the QTP using an interpolation method based on meteorological stations (Wang et al., 2009; You et al., 2011). In the absence of a large, distributed network of meteorological stations, remote sensing becomes a necessary technique.

Optical remote sensing can be used to identify snow cover extent accurately using the normalized difference of snow index (NDSI) method due to its high reflectance in the optical band and low reflectance in the near infrared band (Hall et al., 2002 and 2007). However, the drawback of optical remote sensing is that clouds mask snow data on most the days during the snow season. Therefore, 8-day and 16-day composite snow cover products are produced to remove cloud cover (Hall et al., 2002 and 2007). Daily cloud-free snow cover products were also produced using temporal or spatial interpolation algorithms (Tang et al., 2013; Hall et al., 2010; Gafurov and Bardossy, 2009; Parajka et al., 2010). However, for the strong spatial heterogeneity and rapid snow cover changes across the QTP, interpolation algorithms do not work under conditions of continuous multi-day cloud cover or for large areas. Therefore, in the cloud-covered areas, snow cover derived from passive microwave (PM) remote sensing, which is independent of sunlight, has been used to supplement optical remote sensing (Liang et al., 2008; Gao et al., 2012; Deng et al., 2015). The data from the combination of these two techniques provides information masked by clouds and improves the temporal resolution of snow cover products. Many combined snow cover products have been used in climate change and hydrological analysis (Barnett et al., 2005; Wang et al., 2015). A typical

product is the interactive multisensory snow and ice mapping system (IMS) (Ramsay, 1998). Based on IMS, researchers have observed that snow extent has decreased in the Northern Hemisphere, especially in spring (Brown and Robinson, 2011), snow onset is delayed, the last day of snow is earlier, and number of snow cover days is fewer based on snow cover products (Choi et al., 2010). However, the accuracy of snow cover from PM directly influences the accuracy of the combined snow cover product. In addition, although optical remote sensing is an efficient way to monitor spatial snow cover with high resolution, it cannot penetrate snowpack and obtain snow depth.

PM is the only efficient way to monitor the spatial and temporal variation of snow depth. It is used to identify snow cover based on the volume scattering of snow particles. Brightness temperature emitted from the ground goes through snowpack and is scattered by snow particles. Furthermore, the scatter intensity at low frequency is weaker than that at high frequency, and the difference increases with number of snow particles. Therefore, regional and local snow depths have been retrieved based on the microwave spectral gradient method (Kelly et al., 2003; Pullianen et al., 2006; Dai et al., 2012; Jiang et al., 2014), and these snow depth products have been widely used in climate change and vegetation variation, frozen soil detection, and hydrological cycle studies (Gao et al., 2012; Yu et al., 2013; Xu et al., 2009).

However, there are uncertainties with these snow depth products. The NASA snow water equivalent product derived from Advanced Microwave Scanning Radiometer for Earth Observing System (AMSR-E) generally tends to underestimate snow depth in North America (Tedesco and Narvekar, 2010), but overestimate in China (Dai et al., 2012; Che et al., 2016). Over the QTP, the snow cover was also overestimated by the existing snow products (Frei et al., 2012; Armstrong and Brodzik, 2002). Liquid water within snowpack masks volume scatter, and large grain sizes may contribute more to spectral gradient than snow depth. It is difficult to accurately correct for these snow characteristics at large scale to improve the modelling accuracy of brightness temperature. Some research uses a priori snow characteristics, assimilates snow depth observed at stations, or builds a local empirical relationship between snow depth observations and spectral gradients to improve the snow depth retrieval accuracy in some regions (Dai et al., 2012; Che et al., 2016, 2008; Pullianen, 2006). However, uncertainties still exist for the QTP, which is caused by the coarse spatial resolution of passive microwave remote sensing and the patchy distribution of snow cover. Across the QTP, meteorological stations are rare and mainly distributed in the valley with low elevation. Snow depth observed at these stations does not represent the snow status of the grid they are located on, and so it

is unclear if data assimilation and an empirical equation will work to improve snow depth accuracy. It has also been reported that snow cover across the QTP is overestimated by PM algorithms compared to IMS snow cover products, caused by a thinner atmosphere (Savoie et al., 2009). At present, there is no definitive evaluation of the source of uncertainties or of the accuracy of snow depth products across the QTP, although there has been some comparison to meteorological station observation data (Yang et al., 2015).

Therefore, the purposes of this study are to provide a reliable evaluation or assessment of the ability of passive microwave to detect snow cover and snow depth across the QTP using MODIS snow cover product, in situ and airborne observation data, analyze the cause of uncertainties, and provide reference for the use of PM snow depth data and improvements to the retrieval algorithm for snow depth across the QTP.

2. DATA

2.1 MODIS snow cover fraction

The Terra/Aqua MODIS Level 3, 500m daily snow cover products (MOD10A1 and MYD10A1) were obtained from the National Snow and Ice Data Center (NSIDC) from 1 January, 2003 to 31 December, 2014 (Hall et al., 2006). The snow cover fraction (SCF) product derived from MODIS is generated based on the regression relationship between normalized difference snow index (NDSI) and SCF. The relationship equation is SCF = 0.06 + 1.21 * NDSI, and it was developed over three different snow covered regions. To develop a relationship between NDSI and SCF within a MODIS 500-m pixel, it was necessary to utilize a source of ground truth. In this algorithm, several Landsat scenes covering a wide variety of snow-cover conditions were selected, and every 30-m pixel of Landsat scene was classified as snow or no-snow. The number of snow-cover pixel for Landsat in a MODIS grid and the total number of Landsat pixels in a MODIS grid were calculated. The ratio of them was the ground truth of SCF (Salomonson and Appel, 2004). When the derived snow cover fractions were compared to Landsat-7 Enhanced Thematic Mapper ground-truth observations covering a substantial range of snow cover conditions, the correlation coefficients were near 0.9 and the RMSE were near 0.10 (Salomonson and Appel, 2004 and 2006).

The Cryosphere Discuss., doi:10.5194/tc-2016-262, 2016
Manuscript under review for journal The Cryosphere
Published: 19 December 2016

2.2 Passive microwave brightness temperature and snow depth product

The AMSR-E, which measures twelve bands of six frequencies, was operated from the NASA EOS Aqua Satellite and provided global passive microwave measurements of the earth from June, 2002 to October, 2010. To provide consistency of different frequencies with different footprints, the brightness temperature was resampled to an equal-area scalable earth grid (EASE-Grid) with a resolution of 25 km, approximately equal to 0.1° across the QTP. In this study, the brightness temperature at 18.7 GHz, 36.5 GHz at both vertical and horizontal polarization (TB_{18H}, TB_{18V}, TB_{36H}, TB_{36V}), 23.8 GHz, and 89.0 GHz at vertical polarization (TB_{23V}, TB_{89V}) from 1 January, 2003, to 31 December, 2008, were used to identify snow cover and derive snow depth across the QTP.

The Advanced Microwave Scanning Radiometer-2 (AMSR2) carried on the Global Change Observation Mission (GCOM) was launched on May 18, 2012 (Imaoka et al. 2010), and provided brightness temperature from July 3, 2012. The AMSR2 sensor was the continuation of AMSR-E and has the same channels as the AMSR-E but a slightly smaller footprint. The AMSR2 brightness temperatures from November, 2013 to March, 2014 were used to derive the snow depth in the field experiment areas.

The core principle of retrieving snow depth from passive microwave remote sensing data is that snow particles scatter the microwave signals emitted from the ground, and the brightness temperature of ground declines as it crosses the snowpack. The higher the frequency, the greater the radiation scatters, and more snow particles lead to a larger brightness temperature gradient. Therefore, the spectral gradient, namely the brightness temperature difference between lower frequency and higher frequency is used to derive snow depth. Based on modeling and observation, the 18 GHz (K band) and 36 GHz (Ka band) are the best frequencies for deriving snow depth (Chang et al., 1987; Kelly et al., 2003). The brightness temperature difference between these two frequencies (TBD) has a good relationship with snow water equivalent.

However, frozen soil and cold desert also scatter radiation, and their existence leads to a positive TBD (Grody and Basist, 1996). Therefore, before retrieving snow depth, snow cover must be identified from other scattering sources. In this study, a modified global snow identification method (Che et al., 2008) is used to retrieve snow cover using AMSR-E brightness temperature. The criteria are described as following:

Cold desert: TB_{19V}-TB_{18V} >=18 (K) AND TB_{19V}-TB_{37V}<=10 (K) AND TB_{37V}-TB_{85V}<=10 (K)

The Cryosphere Discuss., doi:10.5194/tc-2016-262, 2016
Manuscript under review for journal The Cryosphere
Published: 19 December 2016

Frozen soil: TB_{19V}-TB_{19H}>=8 (K) AND TB_{19V}-TB_{37V}<=2 (K) AND TB_{37V}-TB_{85V}<=6 (K)

Snow depth (cm) = 0.7*(TB_{18H}-TB_{36H}-5)+offset

2.3 Meteorological station observations of snow depth

Daily snow depths and snow water equivalents were observed at 109 meteorological stations across the QTP with a spatial distributions provided in Fig. 1. Snow depths from meteorological stations were observed daily at 8:00 am using rulers, and the record is the mean value of three individual measurements.

2.4 Field experiments

From 20 November to 7 December, 2013, snow depths were observed along an observation route (Fig. 1, red line). During this period, little snow accumulated; only some patchy snow was distributed which cannot be measured by ruler. From 23 March to 31 March, 2014, snow characteristics were observed along an additional observation route (Fig. 1, blue line). Snow depth was recorded every 5~10 km in the snow-cover area, and snow depths in the transition region were also measured. During this field campaign, 56 snow depths were recorded. From 6 to 25 May, 2014, snow depths were observed along an additional observation route (Fig. 1, green line). During this period, there was no snow distribution except at the tops of mountains, which was not measurable.

The Binggou watershed in the Qilian Mountains, an area of 30 km^2, is located in the northeast of the QTP (Fig. 1, pink polygon), where dense snow depths were measured during the watershed allied telemetry experimental research (WATER) field campaign carried out in March of 2008. During this experiment, 51 snow depths were measured using snow stakes on the 2, 4, 9, 16, 19, 21, 23, and 29 of March and the 1 and 6 of April. On 29 March, 2008, airborne microwave radiometry experiment was carried out, providing brightness temperatures at the 18 and 36 GHz, and 78 snow pits including snow depth, snow density and grain size were observed at four sampling sites (Li et al., 2009; Che et al., 2012). These data were all used to evaluate the identification of snow cover by passive microwave and the accuracy of the satellite-derived snow depth.

The Cryosphere Discuss., doi:10.5194/tc-2016-262, 2016
Manuscript under review for journal The Cryosphere
Published: 19 December 2016

3 Evaluation methods and results

The MODIS snow cover fraction product, meteorological station observations, and field campaign snow depth observations are compared with the AMSR-E/AMSR2 snow cover, and snow depths observed at meteorological stations and field experiments are compared with AMSR-E/AMSR2 snow depths.

3.1 Comparison with MODIS snow cover fraction product

Based on the snow-cover identification algorithm described in section 2.2, the AMSR-E brightness temperatures were used to calculate the TBD, which represents snow depth. MODIS snow cover fractions (SCF) with a resolution of 500 m were resampled to 0.1 °, similar to the AMSR-E resolution across the QTP. For every AMSR-E grid, SCF was recalculated based on the no-cloud MODIS grids (new SCF), and the number of cloud-cover grids in every AMSR-E grid was also recorded. The AMSR-E TBDs were grouped into 5 groups: <=5 K, 5~10 K, 10~15 K, 15~20 K, >20 K, and the new SCFs were divided into six groups: <10 %, 10 %~30 %, 30 %~50 %, 50 %~70 %, 70 %~90 %, >90 %. The frequencies of each SCF with cloud fraction less than 10 % for each TBD group from 2003 to 2007 were computed. The results are described in the TBD-SCF table, which is the basis for determining the likelihood of snow cover for each AMSR-E grid given a TBD. The flowchart for building the TBD-SCF table is provided in Fig. 2.

The frequency histograms of SCF > 10 %, 30 %, 50 %, 70 %, and 90 % were calculated according to the TBD-SCF table (Fig. 3), and the spatial distribution of the frequency of SCF > 10 % corresponding to each TBD group is presented in Fig. 3. If SCF > 10 % was considered as snow cover, grids with TBD more than 20 K showed 4.9 % snow-free area, 82.9 % snow area, and 12.2 % uncertainty area, including 6.1 % high possibility of snow cover area and 6.1 % high possibility of snow-free area. A decrease in TBD causes the certainty ratio to decline and the uncertainty to increase. TBD between 15 and 20 K showed 5.9 % snow-free area, 68.2 % snow-covered area, and 25.9 % uncertainty area. The TBD between 5 and 10 K presented the highest uncertainty. When the TBD is less than 5 K, the QTP is dominated by no snow, and the snow-covered areas are mainly glaciers and lake ice, based on the land cover map. However, there is a large area of uncertainty with a low possibility of snow. Therefore, snow cover is difficult to identify when the TBD is between 5 and 15 K.

If SCF >30 % is considered as snow cover, the uncertainty areas increase when TBD is more than 5 K, but the snow-free areas increase when TBD is less than 5 K. If SCF > 50 % is considered as snow cover, only 3.3 % of the area is definitely

The Cryosphere Discuss., doi:10.5194/tc-2016-262, 2016
Manuscript under review for journal The Cryosphere
Published: 19 December 2016

identified as snow when TBD is between 5 and 10 K, 9.8 % when TBD is between 10 and 15 K. With an increase in TBD, the snow cover areas increase, and the uncertainty area increases. Therefore, although there is no obvious relationship between TBD and snow cover fraction, TBD can reflect snow cover fraction to a certain extent.

With SCF > 0.1 as snow cover and TBD > 5 K is the threshold to identify snow from AMSR-E, the overall accuracy, underestimation, overestimation, commission and omission errors of AMSR-E were analyzed (Fig. 4, Table 1). The overall accuracy is 66.7 % and varies spatially. In this condition, 27.6 % of snow-free areas are misclassified as snow cover (commission), and 47.4 % of snow cover grids are not be detected by AMSR-E (omission); meanwhile, 56.1 % of grids identified as snow covered by AMSR-E were free of snow (overestimation), and 21.1 % of snow-free grids from AMSR-E were in fact covered by snow (underestimation), which is mainly distributed in the lake and glacier areas. The lowest accuracy occurs in the northwest area of the QTP, where commission error reaches up to 0.6-0.8. Although the overall accuracy for the cold desert areas is more than 0.8, in most of these areas, the omission error is also up to 0.8, which means that 80 % of snowfall cannot be detected by AMSR-E. In these areas, snowfall is a rare event, and snow depth is low, which changed TBD slightly, so TBD > 5 K does identify the shallow snow in these areas. The high overall accuracy of these areas is due to the large number of snow-free days. In the mountainous areas of southeast and northeast Qilian and the northwest area of the QTP, AMSR-E showed high overestimation and commission errors.

The snow cover accuracy of AMSR-E varies spatially and depends on the snow cover fraction calculated based on the MODIS SCF products. The overall accuracy was over 60 % in most of areas, but omission and overestimation errors also exist in large areas with shallow snow.

3.2 Comparison with observed snow depth

Daily snow depths from meteorological stations from 2003 to 2007, snow depth from the three observation routes in 2013 and 2014, and snow depth observed at the Binggou watershed in 2008 were compared with the snow cover and snow depth derived from AMSR-E or AMSR2.

The Cryosphere Discuss., doi:10.5194/tc-2016-262, 2016
Manuscript under review for journal The Cryosphere
Published: 19 December 2016

3.2.1 Comparison with meteorological station observation

Snow cover conditions were derived from AMSR-E or AMSR2 at grids that contained meteorological stations and were compared with observations. The comparison results showed that the overall accuracy of AMSR-E snow cover is 77.6 %, where 40.6 % of snow covered points were not detected by AMSR-E, and 21.2 % of snow-free points were misclassified as snow covered by AMSR-E. The overestimate and underestimate are 83.8 % and 3.5 %, respectively. A meteorological station may not represent the status of an entire PM grid in the complex territorial region, therefore snow cover fractions in the PM grid were derived based on MODIS snow cover production and compared with meteorological observations. The results showed that when MODIS SCF was greater than 10 %, only 22.4 % of snow depth observations were greater than 0 cm, a MODIS SCF greater than 30 % corresponded to 39.8 % of observations greater than 0 cm, and a MODIS SCF greater than 50 % corresponded to 54.9 % of observations greater than 0 cm. Therefore, although station snow observations are in good agreement with the snow cover MODIS grid (Yang et al., 2015), they cannot represent the snow cover in a PM grid across the QTP.

Due to the disagreement between the PM grid and station-based snow cover measurements, snow depths from stations and AMSR-E greater than 0 were compared (Fig. 5). The results showed that AMSR-E overestimates snow depths across the QTP, in agreement with results of Yang et al. (2015). The mean snow depth, bias and RMSE are 4.0 cm, -0.45 cm and 6.7 cm, respectively, and the relative error is 131.4 %. From Fig. 5, snow depths greater than 20 cm were always underestimated by AMSR-E, caused primarily by the data that came from the Nyalam station (Id: 55655) located in the Himalaya Mountains. If the data at this station are removed from the statistics, the mean snow depth, the bias and RMSE are 3.5 cm, 1.7 cm and 5.5 cm 4.0 cm, respectively, and the relative error is 152.3 %.

3.2.2 Comparison with field observations

Observations from December of 2013 and May of 2014 indicated sparse snow along the observation route, a result also shown by AMSR2. During the observations in March of 2014, 56 points of snow depth were measured within 33 AMSR2 grids (Figure 1). Comparison between ground observations and retrievals from AMSR2 indicates that the retrieval accuracy of snow cover from AMSR2 is 94 %,. The average snow depth of observed measurements is 6.71 cm, the bias between them is 0.27 cm, RMSE is 5.4 cm, and the correlation coefficient is 0.574 (Fig. 6 a).

The Cryosphere Discuss., doi:10.5194/tc-2016-262, 2016
Manuscript under review for journal The Cryosphere
Published: 19 December 2016

In 2008, there were five groups of snow depth observations and a total 51 points, all within an AMSR-E grid in the Binggou watershed (Che et al., 2012). The average snow depths of the 51 points for the 2, 4, 9, 16, 19, 21, 23, and 29 March and 1 and 6 April were 18.2 cm, 15.5 cm, 21.5 cm, 20.0 cm, 24.6 cm, 21.5 cm, 24.2 cm, 18.0 cm and 14.4 cm. Snow depths varied between 0 and 60 cm. Compared with these snow depths, the snow depths derived from AMSR-E generally present underestimation; the bias is -10.0 cm, and the RMSE is 10.5 cm (Fig. 6 b). Therefore, based on the field investigation, snow cover can be detected accurately by AMSR-E because of deep snowpack, but the accuracy of snow depth retrieval is low. Although the observations in the Binggou watershed were dense, due to the large spatial variation in snow depth and topography, an average snow depth may not represent the snow depth of a whole grid. Che et al. (2008) analyzed the relationship between snow depth distribution, elevation, and directional aspect using the snow depth estimated from airborne radiometer data with a footprint of 16-39 m at 36 GHz and 158-395m at 18 GHz. The authors found that snow cover was primarily distributed in a northerly aspect. The snow cover fractions across the QTP derived from the MODIS snow cover product are 52 %, 35 %, 45 %, 34 %, 36 %, 46 %, 42 %, 17 % and 21 % for 2 March, 4 March, 9 March, 16 March, 21 March, 23 March, 29 March, 1 April and 6 April, respectively, and the average snow depths in the AMSR-E footprint are calculated by multiplying the snow cover fraction by the observed mean snow depth. The average snow depths in the AMSR-E footprint are compared with the derived snow depth, exhibiting average snow depth, bias, RMSE, and absolute relative error of 7.4 cm, -0.4 cm, 2.2 cm, and 29.5 %, respectively (Fig. 6 b).

Therefore, the spatial inhomogeneity of snow depth is the main contributor to the difference between satellite and in situ observation. Snow depth in a PM grid is reflected in the dense sample and snow cover fraction across the QTP.

4. Sources of error

According to the comparison in section 4, PM remote sensing overestimated the snow cover extent in some areas and omitted snow cover in the shallow snow areas. Here, we discuss potential reasons for the misclassification.

4.1 Cold desert

The omissions mainly appeared in the desert areas, with the exception of the lake ice areas. In these areas, there is no heavy snow, and the snow depth is usually less than 5 cm. The fallen snow melts quickly in a few days, resulting in a small TBD

The Cryosphere Discuss., doi:10.5194/tc-2016-262, 2016
Manuscript under review for journal The Cryosphere
Published: 19 December 2016

change. Take the Tuotuohe station (Id:56004) for example; this station is located in a desert area, and during the winter, sand scatters the microwave signal and presents weak scattering features. The TBD contributed by sand is less than 5 K, but even if the sand-covered land was covered by snow, the TBD did not increase and remained less than 5 K. Liquid water melted from snow cover will even decrease the TBD. The criterion for cold desert identification presented in the section 2.2 removes not only the desert as a scatterer but also the snowpack.

4.2 Soil temperature

TB_{36V} is sensitive to topsoil temperature (Holmes et al., 2009; Zeng et al., 2015). Statistical analysis between TBD (K) and TB_{36V} at 109 stations showed that TBD has a significant negative correlation with TB_{36V} (Fig. 8 a), but no obvious relationship with snow cover fractions. Batang station (Id: 56247) is a typical station, where snowfall is rare, the PM grid of this station was seldom covered by snow, and the snow cover fraction in the AMSR-E grid was greater than 10 % on only a few days based on MODIS snow cover fraction products. The temporal variation in TB_{36V}, TBD, and snow depth at this station also indicates that a decrease of TB_{36V} is accompanied by a TBD increase to over 5 K with a snow depth of 0 cm (Fig. 8 b). TB_{36V} and TBD have a highly negative correlation (Fig. 8 c). Therefore, the ground temperature is the main contributor to the increase in TBD.

The penetrability of 18 GHz and 36 GHz are different and depend on the soil features. In the summer, the brightness temperature at 18 GHz and 36 GHz is emitted from the ground surface, but with decrease of temperature and soil freezing, the penetration depth of 18 GHz is larger than the 36 GHz. The higher temperature at deeper place contributes to the brightness temperature of the 18 GHz and lower temperature close to the surface contributes to the brightness temperature of the 36 GHz. Furthermore, the 36 GHz is sensitive to both ground surface temperature and snowpack, but ground surface temperature is also influenced by snowpack. Because of snowpack thermal insulation and thermal transfer of soil, ground surface temperature may stay high when covered by snow. As the brightness temperature of the Ka band emitted from ground increases, it is also reduced by snowpack when arriving at sensor. Therefore, it is difficult to discriminate what is the main factor to cause the decrease of brightness temperature at 36 GHz.

Therefore, we believe the ground feature is the main resource of errors. Accurately modelling the brightness temperature of different bands emitted from the ground is key to improving the accuracy of snow cover detection.

The Cryosphere Discuss., doi:10.5194/tc-2016-262, 2016
Manuscript under review for journal The Cryosphere
Published: 19 December 2016

4.3 Atmospheric correction

Thinner atmosphere across the QTP was the hypothesized cause of overestimation of snow depth from PM remote sensing (Savoie et al., 2009; Qiu et al., 2009). Prior researchers assumed that general algorithms built based on satellite brightness temperature and ground snow depth implicitly accounted for the presence of an atmosphere. In this study, we used the atmosphere correction method developed in Savoie et al. (2009) to adjust the brightness temperature of QTP to that of a lower elevation and then derive the snow cover from AMSR-E from 2003 to 2007. The derived snow cover was compared with snow cover fraction estimates from MODIS. The comparison results indicated that the overall accuracy improved from 66.7 % to 72.2 %, the commission error decreased from 27.6 % to 14.2 %, and overestimation error decreased from 56.1 % to 46.8 %, but the omission error increased from 47.4 % to 60.8 %, meaning that an additional 13.4 % of snow cover was not detected (Table 2). If the TBD threshold used for identifying snow cover changed to 1 or 2 K, then the overall accuracy, overestimation and omission would exhibit the same change in trend as with an atmospheric correction.

4.4 Spatial resolution and topography

The footprint of airborne radiometer data in the Binggou watershed experiment were 16-39 m at Ka band and 158-395 m at 18GHz. Considering the speed of the aircraft and interval time of radiometers, the brightness temperatures of both frequencies were gridded at 90 m resolution. The observed points were distributed in separate grids. Che et al. (2008) used an MEMLS model to simulate the brightness temperature of snow cover for each observation point and developed a snow depth retrieval algorithm in the Binggou watershed. The mean absolute and relative errors of snow depth estimates were approximately 3.5 cm and 14.8 % for the stake and sampling-site regions. The mean absolute and relative errors for AMSR-E are 2.0 cm and 29.5 %, respectively, in the AMSR-E grid. Although the derived snow depths from airborne and satellite radiometry agreed with each other, the average airborne brightness temperature and AMSR-E brightness temperature at 36GHz presented a large bias.

The satellite and airborne radiometers have similar radiation characteristics and were all well calibrated. The aircraft flew at an altitude of 5000 m, where atmospheric influence on the airborne and satellite brightness temperatures should be the same. The difference between the airborne and satellite data is the spatial resolution, overpass time and incidence angle. In the Binggou watershed, snow cover presented strong heterogeneity. Fifty-one snow stakes covered 51 airborne grids located on

The Cryosphere Discuss., doi:10.5194/tc-2016-262, 2016
Manuscript under review for journal The Cryosphere
Published: 19 December 2016

seven MODIS grids. In contrast, the satellite grid only overlapped with a small part of the PM grid (Fig. 9). Fifty-one snow depths varied between 0 and 60 cm, which can be detected by airborne radiometry, but for MODIS, they were all covered by snowpack. For the AMSR-E grid, they did not reflect snow distribution, although they were measured in different directional aspects and elevations.

Airborne experiments were carried out in daytime, which was closer to the ascending overpass of AMSR-E. The ascending TBD was less than 2 K, and the descending TBD was approximately 11 K, as presented in Fig. 9. In daytime, the snow cover melted in some areas, which led to spatially variant liquid water content and likely caused some of the differences between the airborne and satellite brightness temperature. In addition, the scan areas of the airborne radiometry were not identical to the satellite observations, which is an additional cause of the large gap between the airborne and satellite brightness temperatures for heterogeneous distribution of snow cover in the Binggou watershed.

4.5 Snow characteristics

Based on spectral gradient algorithms, derived snow depths are closely related to TBD. However, TBD is not only influenced by snow depth but also other snow characteristics, in particular, snow grain size. At the beginning of snowfall, snow grain size is small and the snowpack is transparent for microwave, so passive microwave remote sensing underestimates the snow depth in this period. With increasing snow age, grain size increases, which contributes to TBD, so snow depth may be overestimated by passive microwave remote sensing. Therefore, accurately monitoring the snow depth using passive microwave requires a priori knowledge of snow characteristics (Dai et al., 2012; Che et al., 2016; Huang et al., 2012; Tedesco and Narvekar, 2010). In this study, 16 % of snow depths greater than 10 cm observed at meteorological stations were misclassified as snow-free grids by AMSR-E. This misclassification occurred in the areas of sparse snow, where heavy snowfall occurred occasionally but melted in 1-3 days. During the field campaign in March 2014, snowpack measured on 23 March was fresh snow but was misclassified as no snow cover.

Therefore, accurately modeling the ground brightness temperature at both frequencies and snow characteristics are two key factors for improving snow depth and snow cover accuracy of PM. However, the strong heterogeneity of snow distribution over the QTP requires a retrieval algorithm with high resolution.

The Cryosphere Discuss., doi:10.5194/tc-2016-262, 2016
Manuscript under review for journal The Cryosphere
Published: 19 December 2016

5 Conclusions

Although satellite-based passive microwave brightness temperature data have been used to monitor global and local snow depth since the 1980s, the accuracy of snow cover and snow depth across the QTP derived from passive microwave remote sensing was still largely unknown. There are no prior studies that provided a detailed evaluation on the products of PM across the QTP, resulting in difficulties for users in selecting appropriate products. In this study, snow cover fractions derived from MODIS, meteorological station snow depth, in situ snow depth, and airborne snow depth were combined to evaluate the ability of AMSR-E to identify snow cover and snow depth and to analyze the sources of error.

The results show that the overall accuracy of snow cover derived from passive microwave remote sensing across the QTP varies spatially and depends on snow cover fraction, based on MODIS snow cover fraction. Commission errors were mainly distributed in the northwest and southeast where ground temperature was low, and omission errors were found in the cold desert areas with sparse snowfall. If snow cover fraction greater than 0.1 in a grid was classified as covered by snow, the overall accuracy of snow cover from AMSR-E was 66.7 %. AMSR-E misclassified 27.6 % of snow-free grids as snow covered, 47.4 % of snow-covered grids cannot be detected by AMSR-E, 56.1 % of grids were overestimated, and 21.1 % of grids were underestimated.

Although snow observations at meteorological stations agree with MODIS observations, they do not represent snow cover at PM grids. Therefore, it is unreasonable to use station observations to assess the snow cover and snow depth monitoring ability of PM across the QTP. Comparison between snow observation from field experiments and AMSR-E/AMSR2 showed that the snow depth bias and relative errors along the field campaigns' observation routes were less than that for the Binggou watershed. However, when compared with area-weighted snow depth, the derived snow depth has a relative error of 29.5 %, less than the observation routes, and the results agree with the airborne observation from the Binggou watershed. Therefore, assessing the brightness temperature in the PM grid is an urgent problem for validating snow depth products from PM.

Ground temperature decreases changes the TBD and cause an overestimation of snow cover, and it is difficult to discriminate the weak scattering of shallow fresh snow from a cold desert. The mountainous topography and the coarse resolution of PM resulted in the large disagreement between the snow depth derived from AMSR-E and in situ observations or airborne radiometry. Therefore, accurately monitoring the spatiotemporal distribution of snow depth across the QTP requires improving the retrieval accuracy of PM as well as the spatial resolution. A new snow depth retrieval algorithm is suggested to combine optical remote sensing, PM and operational station observations.

Acknowledgements

This study was supported by the National Natural Science Foundation of China (91547210, 41401414 and 41271356), the China State Key Basic Research Project (2013CBA01802), and the Chinese Academy of Sciences Project (KJZD-EW-G03).

References

Armstrong, R.L. and Brodzik, M.J.: Hemispheric-scale comparison and evaluation of passive-microwave snow algorithms, Ann Glaciol, 34, 87-92, 2002.

Barnett, T.P., Adam, J.C. and Lettenmaier, D.P.: Potential impacts of a warming climate on water availability in snow-dominated regions, Nature, 438(7066), 303-309, 2005.

Brown, R.D. and Robinson, D.A.: Northern Hemisphere spring snow cover variability and change over 1922-2010 including an assessment of uncertainty, Cryosphere, 5(1), 219-229, 2011.

Bulygina, O.N., Razuvaev, V.N. and Korshunova, N.N.: Changes in snow cover over Northern Eurasia in the last few decades, Environ Res Lett, 4(4), 2009.

Chang, A., Foster J. and Hall D.: Nimbus-7 SMMR derived global snow cover parameters, Ann Glaciol, 9(9), 39-44, 1987.

Che, T., Dai, L.Y., Wang, J., Zhao, K. and Liu, Q: Estimation of snow depth and snow water equivalent distribution using airborne microwave radiometry in the Binggou Watershed, the upper reaches of the Heihe River basin, Int J Appl Earth Obs, 17: 23-32, 2012.

Che, T., Dai, L.Y., Zheng, X.M., Li, X.F.and Zhao, K.: Estimation of snow depth from passive microwave brightness temperature data in forest regions of northeast China, Remote Sens Environ, 183, 334-349, 2016.

Che, T., Li, X., Jin, R., Armstrong, R. and Zhang, T.J.: Snow depth derived from passive microwave remote-sensing data in China, Ann Glaciol, 49, 145-154, 2008.

Choi, G., Robinson, D.A. and Kang, S.: Changing Northern Hemisphere snow seasons, J. Climate 23(19), 5305–5310, 2010.

Cohen, J.: Snow cover and climate. Weather, 49, 150-156, 1994.

Dai, L.Y. and Che, T.: Spatiotemporal variability in snow cover from 1987 to 2011 in northern China, J Appl Remote Sens, 8, 2014.

Dai, L.Y., Che, T., Wang, J. and Zhang, P.: Snow depth and snow water equivalent estimation from AMSR-E data based on a priori snow characteristics in Xinjiang, China, Remote Sens Environ, 127: 14-29, 2012.

Deng, J., Huang, X. and Feng, Q.: Toward Improved Daily Cloud-Free Fractional Snow Cover Mapping with Multi-Source Remote Sensing Data in China, Remote Sens, 7(6): 6986-7006, 2015.

Frei, A. et al., 2012. A review of global satellite-derived snow products, Adv Space Res, 50(8), 1007-1029.

Gafurov, A., Bardossy, A., 2009. Cloud removal methodology from MODIS snow cover product, Hydrol Earth Syst Sc, 13(7), 1361-1373.

Gafurov, A., Vorogushyn, S. and Farinotti, D.: Snow-cover reconstruction methodology for mountainous regions based on historic in situ observations and recent remote sensing data, Cryosphere, 9(2): 451-463, 2015.

Gao, J., Williams, M.W., Fu, X.D., Wang, G.Q. and Gong, T.L.: Spatiotemporal distribution of snow in eastern Tibet and the response to climate change, Remote Sens Environ, 121, 1-9, 2012.

Grody, N.C. and Basist, A.N.: Global identification of snow cover using SSM/I measurements, IEEE T Geosci Remote, 34, 237-249, 1996.

Hall, D.K. and Riggs, G.A.: Accuracy assessment of the MODIS snow products, Hydrol Process, 21(12), 1534-1547, 2007.

Hall, D.K., Riggs, G.A., Foster, J.L. and Kumar, S.V.: Development and evaluation of a cloud-gap-filled MODIS daily snow-cover product, Remote Sens Environ, 114(3): 496-503, 2010.

Hall, D.K., Riggs, G.A., Salomonson, V.V., DiGirolamo, N.E.and Bayr, K.J.: MODIS snow-cover products, Remote Sens. Environ. 83(1–2), 181–194, 2002.

Holmes, T.R.H., De Jeu, R.A.M., Owe, M. and Dolman, A.J.: Land surface temperature from Ka band (37 GHz) passive microwave observations, J Geophys Res-Atmos, 114, 2009.

Huang, C.L., Margulis, S.A., Durand, M.T. and Musselman, K.N.: Assessment of Snow Grain-Size Model and Stratigraphy Representation Impacts on Snow Radiance Assimilation: Forward Modeling Evaluation. IEEE T Geosci Remote, 50(11), 4551-4564, 2012.

Imaoka, K., Kachi, M. and Murakami, H.:. Global Change Observation Mission (GCOM) for monitoring carbon, water cycles, and climate change, Proc. IEEE, vol. 98, no. 5, pp. 717–734, May 2010.

Immerzeel, W.W., Droogers, P., de Jong, S.M., Bierkens, M.F.P.: Large-scale monitoring of snow cover and runoff simulation in Himalayan river basins using remote sensing, Remote Sens Environ, 113(1), 40-49, 2009.

Immerzeel, W.W., van Beek, L.P.H. and Bierkens, M.F.P.: Climate Change Will Affect the Asian Water Towers, Science, 328(5984),1382-1385, 2010.

Jiang, L.M., Wang, P., Zhang, L.X., Yang, H. and Yang, J.T.: Improvement of snow depth retrieval for FY3B-MWRI in China, Sci China Earth Sci, 57(6), 1278-1292, 2014.

Kang, S., Xu, Y., and You, Q.: Review of climate and cryospheric change in the Tibetan Plateau, Environ Res Lett, 5(1), 2010.

Kelly, R.E., Chang, A.T., Tsang, L., Foster, J.L.: A prototype AMSR-E global snow area and snow depth algorithm, IEEE T Geosci Remote, 41(2), 230-242, 2003.

Li, X., Li, X.W. and Li, Z.Y.: Watershed Allied Telemetry Experimental Research, J Geophys Res-Atmos, 114, 2009.

Liang, T.G., Huang, X.D and Cai, X.W.: An application of MODIS data to snow cover monitoring in a pastoral area: A case study in Northern Xinjiang, China, Remote Sens Environ, 112(4), 1514-1526, 2008.

Lu, J.M., Ju, J.H., Kim, S.J., Ren, J.Z. and Zhu, Y.X.: Arctic Oscillation and the autumn/winter snow depth over the Tibetan Plateau, J Geophys Res-Atmos, 113(D14), 2008.

Parajka, J., Pepe, M., Rampini, A., Rossi, S. and Bloschl, G.: A regional snow-line method for estimating snow cover from MODIS during cloud cover, J Hydrol, 381(3-4), 203-212, 2010.

Pulliainen, J.: Mapping of snow water equivalent and snow depth in boreal and sub-arctic zones by assimilating space-borne microwave radiometer data and ground-based observations, Remote Sens Environ, 101(2), 257-269, 2006.

Qiu, Y.B., Shi, J.C. and Lemmetyinen, J.: The Atmosphere Influence to Amsr-E Measurements over Snow-Covered Areas: Simulation and Experiments, Ieee International Geoscience and Remote Sensing Symposium, 1-5, 861-864, 2009.

Ramsay, B.H.: The interactive multisensor snow and ice mapping system, Hydrol Process, 12(10-11),1537-1546, 1998.

Salomonson, V.V. and Appel, I.:Estimating fractional snow cover from MODIS using the normalized difference snow index, Remote Sens Environ, 89(3), 351-360, 2004.

Salomonson, V.V. and Appel, I.: Development of the Aqua MODIS NDSI fractional snow cover algorithm and validation results, IEEE T Geosci Remote, 44(7), 1747-1756, 2006.

Savoie, M.H., Armstrong, R.L., Brodzik, M.J. and Wang, J.R.: Atmospheric corrections for improved satellite passive microwave snow cover retrievals over the Tibet Plateau, Remote Sens Environ, 113(12), 2661-2669, 2009.

Shi, H.X. and Wang, C.H.: Projected 21st century changes in snow water equivalent over Northern Hemisphere landmasses from the CMIP5 model ensemble, Cryosphere, 9(5), 1943-1953, 2015.

Tang, Z.G., Wang, J., Li, H.Y., Yan, L.L.: Spatiotemporal changes of snow cover over the Tibetan plateau based on cloud-removed moderate resolution imaging spectroradiometer fractional snow cover product from 2001 to 2011, J Appl Remote Sens, 7, 2013.

Tedesco, M. and Narvekar, P.S.: Assessment of the NASA AMSR-E SWE Product, IEEE J-Stars, 3(1), 141-159, 2010.

Wang, C., Wang Z. and Cui Y.: Snow Cover of China during the Last 40 Years: Spatial Distribution and Interannual Variation, Journal of Glaciology and Geocryology, 31(2), 301-310, 2009 (in Chinese).

Wang, W., Huang, X.D., Deng, J., Xie, H.J., Liang, T.G.: Spatio-Temporal Change of Snow Cover and Its Response to Climate over the Tibetan Plateau Based on an Improved Daily Cloud-Free Snow Cover Product, Remote Sens-Basel, 7(1), 169-194, 2015.

Wu, T.W. and Qian, Z.A.: The relation between the Tibetan winter snow and the Asian summer monsoon and rainfall: An observational investigation, J Climate, 16(12), 2038-2051, 2003.

Xu, C.C., Chen, Y.N and Hamid, Y.: Long-term change of seasonal snow cover and its effects on river runoff in the Tarim River basin, northwestern China, Hydrol Process, 23(14), 2045-2055, 2009.

Xu, X.D., Lu, C.G., Shi, X.H. and Gao, S.T.: World water tower: An atmospheric perspective, Geophys Res Lett, 35(20), 2008.

Yang, J.T., Jiang, L.M.M and Menard, C.B. : Evaluation of snow products over the Tibetan Plateau, Hydrol Process, 29(15), 3247-3260, 2015.

You, Q. L., Kang, S.C. and Ren, G.Y.: Observed changes in snow depth and number of snow days in the eastern and central Tibetan Plateau, Clim Res, 46(2), 171-183, 2011.

Yu, Z., Liu, S.R.and Wang, J.X.: Effects of seasonal snow on the growing season of temperate vegetation in China, Global Change Biol, 19(7), 2182-2195, 2013.

Zeng, J.Y., Li, Z., Chen, Q. and Bi, H.Y.: Method for Soil Moisture and Surface Temperature Estimation in the Tibetan Plateau Using Spaceborne Radiometer Observations, IEEE Geosci Remote S, 12(1), 97-101, 2015.

Zhang, Y.S., Li, T. and Wang, B.: Decadal change of the spring snow depth over the Tibetan Plateau: The associated circulation and influence on the East Asian summer monsoon, J Climate, 17(14), 2780-2793, 2004.

Zhong, X., Zhang, T. and Wang, K.: Snow density climatology across the former USSR, Cryosphere, 8(2), 785-799, 2014.

The Cryosphere Discuss., doi:10.5194/tc-2016-262, 2016
Manuscript under review for journal The Cryosphere
Published: 19 December 2016

List of Table captions

Table 1 Errors in derived snow cover from AMSR-E based on MODIS snow cover fraction and meteorological stations.

Table 2 Errors in snow cover derived from AMSR-E data and atmosphere corrected AMSR-E data over the QTP, based on MODIS snow cover fraction.

The Cryosphere Discuss., doi:10.5194/tc-2016-262, 2016
Manuscript under review for journal The Cryosphere
Published: 19 December 2016

Table 1 Errors in derived snow cover from AMSR-E based on MODIS snow cover fraction and meteorological stations.

	Overall accuracy	Commission	Omission	Overestimation	Underestimation
MODIS snow cover fraction	66.7 %	27.6 %	47.4 %	56.1 %	21.1 %
Meteorological stations	77.6 %	21.2 %	40.6 %	83.8 %	3.5 %

5

Table 2 Errors in snow cover derived from AMSR-E data and atmosphere corrected AMSR-E data over the QTP, based on MODIS snow cover fraction.

	Overall accuracy	Commission	Omission	Overestimation	Underestimation
Original	66.7 %	27.6 %	47.4 %	56.1 %	21.1 %
After atmosphere correction	72.2 %	14.2 %	60.8 %	46.8 %	22.6 %

The Cryosphere Discuss., doi:10.5194/tc-2016-262, 2016
Manuscript under review for journal The Cryosphere
Published: 19 December 2016

The Cryosphere Discussions
Open Access
EGU

List of Figure captions

Fig. 1. Distribution of Meteorological stations, the location of Binggou watershed, and three snow observation routes described in the text overlaid on a digital elevation model for elevation and topography of the QTP.

Fig. 2. Flowchart for building the TBD-SCF table, which provides the relationship between snow cover fraction (SCF) and passive microwave brightness temperature difference (TBD). The SCF of the PM grid was calculated based on the MOD10A and MYD10A products from 2003 to 2007, and TBD was computed using AMSR-E brightness temperature at 18 and 36 GHz for horizontal polarization from 2003 to 2007.

Fig. 3. Spatial distribution of frequency of SCF greater than 10 % across the QTP and histograms of frequency for each SCF group. (a) TBD > 20 K, (b) 15 K < TBD <= 20 K, (c) 10 K < TBD <= 15 K, (d) 5 K < TBD < 10 K, (e) TBD<=5 K

Fig. 4. Spatial distributions of the general accuracy (a) omission errors (b) commission errors (c) underestimation errors (d) and overestimation errors (e) of AMSR-E across the QTP.

Fig. 5. Scatter plot of snow depths observed at meteorological stations and those derived from the AMSR-E from 2003 to 2007.

Fig.6. Comparison between measured snow depth and estimated snow depth from AMSR-E/AMSR2, (a) for March, 2014 along the observation route, (b) for March, 2008 in the Binggou watershed: bar graph of observed snow depth, area-weighted observed snow depth, and estimated snow depth from AMSR-E, and line graph of snow cover fractions on different days.

Fig. 8. Relationship between TBD and TB_{36V} at all stations (a) and Batang station (Id: 56247) (c), and the temporal variation of TB_{36V}, TBD, and snow depth observed at Batang station (b).

Fig. 9. Distribution of snow cover fraction derived from MODIS products in the Binggou watershed, locations of snow stakes set during the Binggou watershed experiment, and the brightness temperature difference between the 18 GHz and 36 GHz from AMSR-E.

The Cryosphere Discuss., doi:10.5194/tc-2016-262, 2016
Manuscript under review for journal The Cryosphere
Published: 19 December 2016

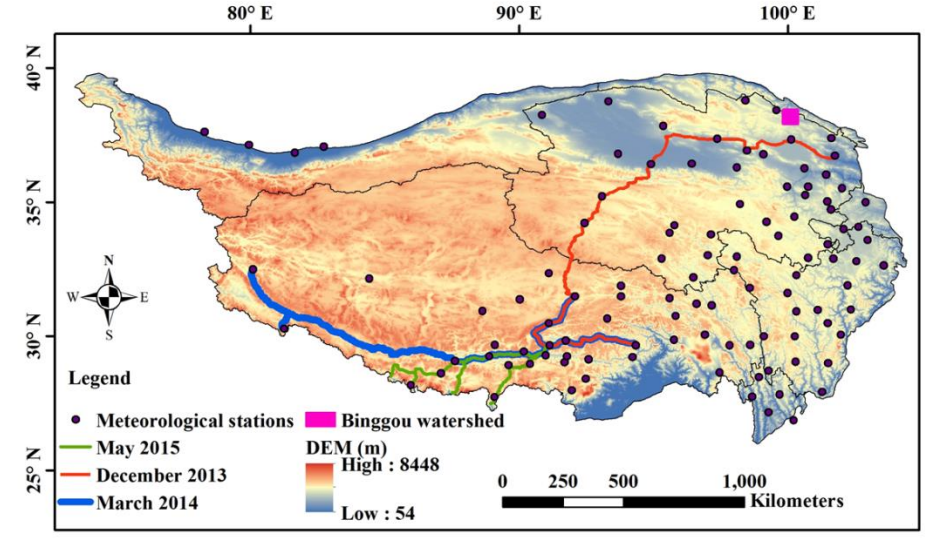

Fig. 1. Distribution of Meteorological stations, the location of Binggou watershed, and three snow observation routes described in the text overlaid on a digital elevation model for elevation and topography of the QTP.

The Cryosphere Discuss., doi:10.5194/tc-2016-262, 2016
Manuscript under review for journal The Cryosphere
Published: 19 December 2016

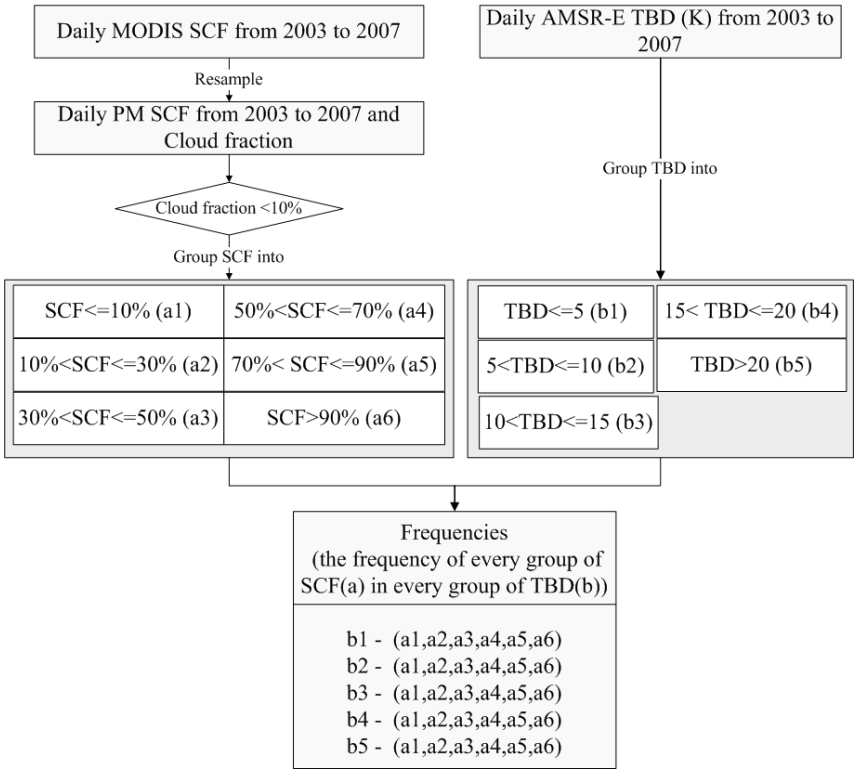

Fig. 2. Flowchart for building the TBD-SCF table, which provides the relationship between snow cover fraction (SCF) and passive microwave brightness temperature difference (TBD). The SCF of the PM grid was calculated based on the MOD10A and MYD10A products from 2003 to 2007, and TBD was computed using AMSR-E brightness temperature at 18 and 36 GHz for horizontal polarization from 2003 to 2007.

The Cryosphere Discuss., doi:10.5194/tc-2016-262, 2016
Manuscript under review for journal The Cryosphere
Published: 19 December 2016

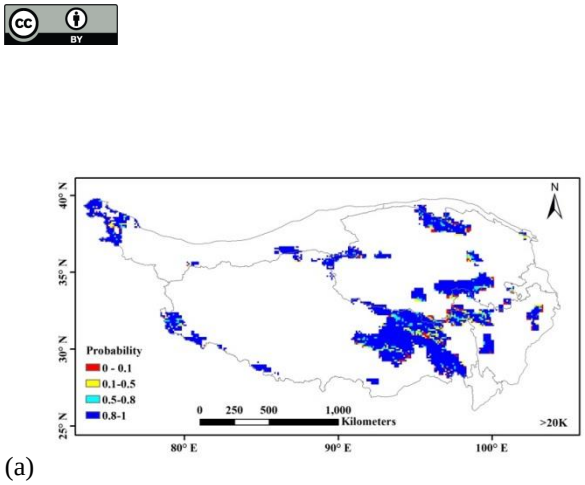

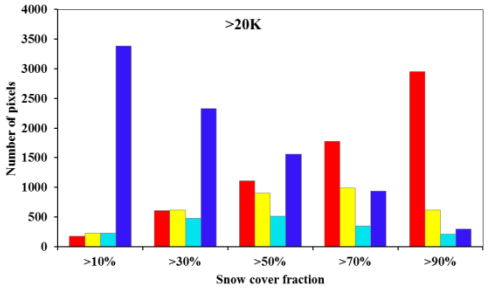

(a)

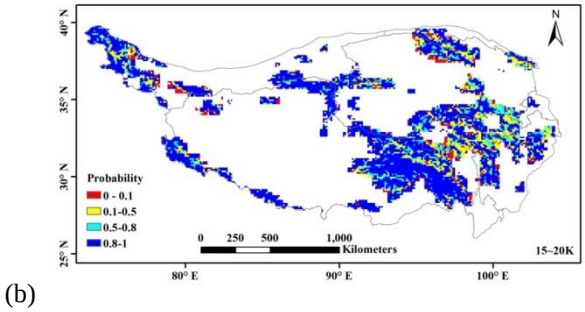

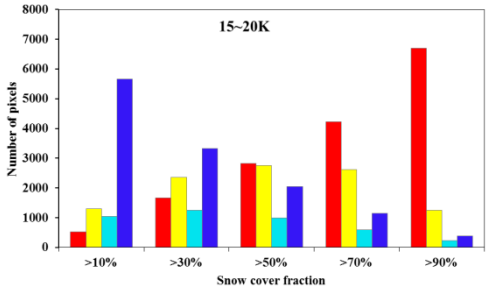

(b)

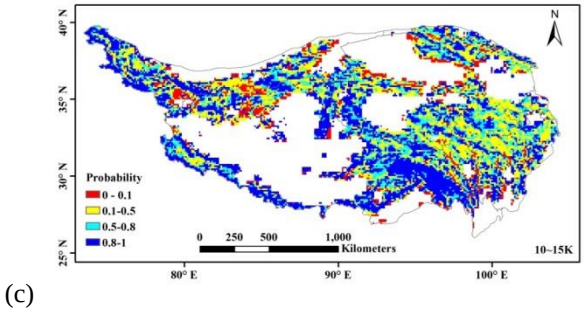

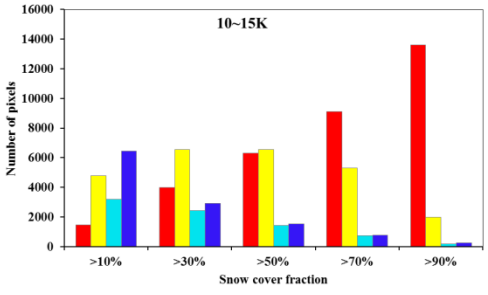

(c)

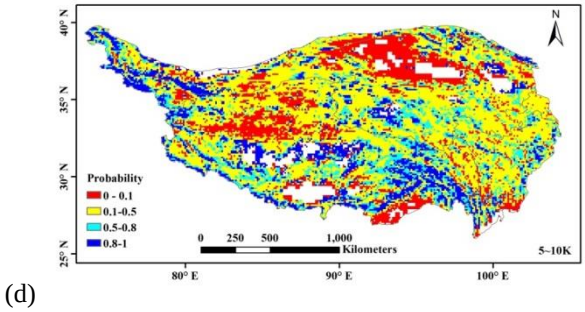

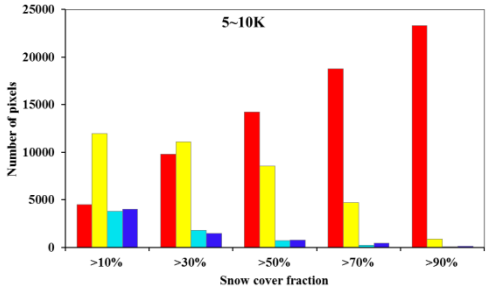

(d)

The Cryosphere Discuss., doi:10.5194/tc-2016-262, 2016
Manuscript under review for journal The Cryosphere
Published: 19 December 2016

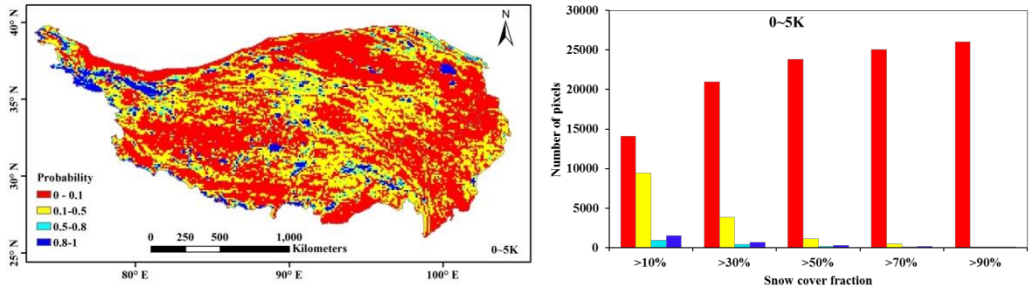

(e)

Fig. 3. Spatial distribution of frequency of SCF greater than 10 % across the QTP and histograms of frequency for each SCF group. (a) TBD > 20 K, (b) 15 K < TBD <= 20 K, (c) 10 K < TBD <= 15 K, (d) 5 K < TBD < 10 K, (e) TBD<=5 K

The Cryosphere Discuss., doi:10.5194/tc-2016-262, 2016
Manuscript under review for journal The Cryosphere
Published: 19 December 2016

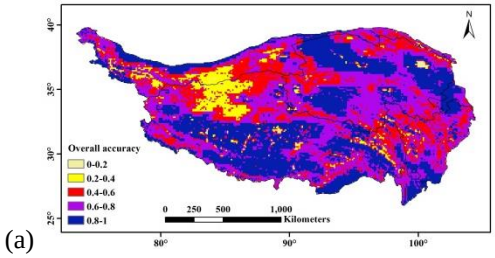

(a)

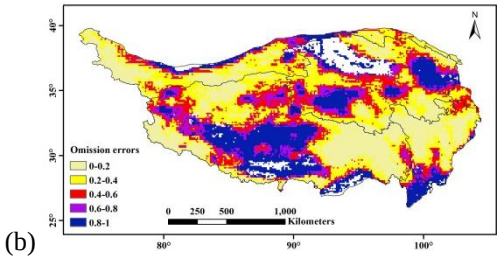

(b)

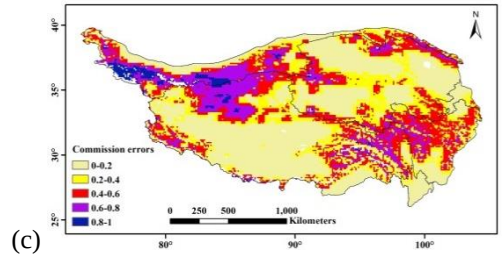

(c)

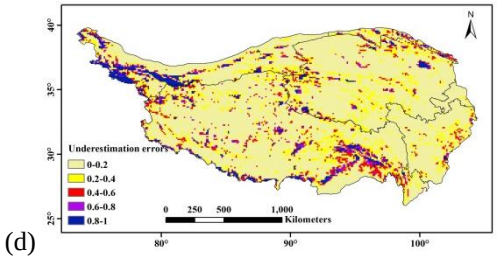

(d)

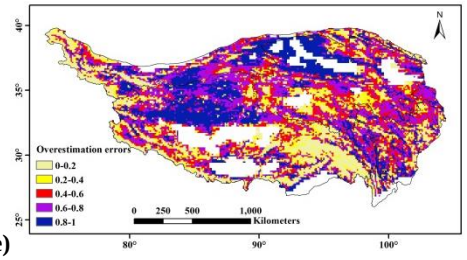

(e)

Fig. 4. Spatial distributions of the general accuracy (a) omission errors (b) commission errors (c) underestimation errors (d) and overestimation errors (e) of AMSR-E across the QTP.

The Cryosphere Discuss., doi:10.5194/tc-2016-262, 2016
Manuscript under review for journal The Cryosphere
Published: 19 December 2016

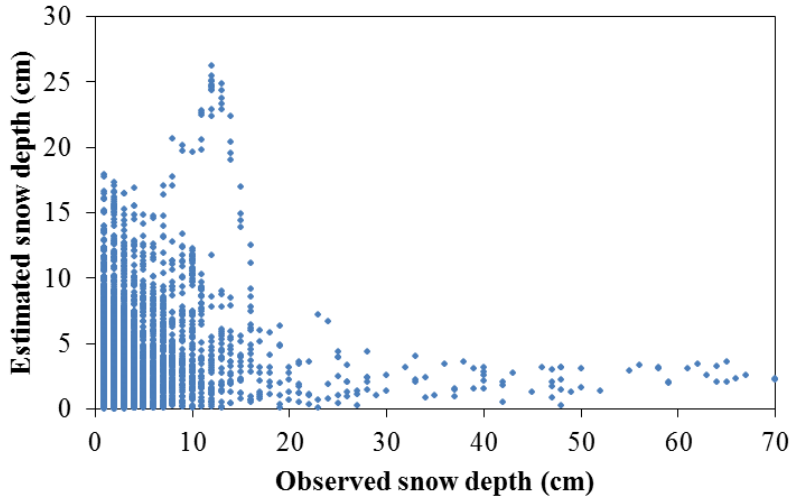

Fig. 5. Scatter plot of snow depths observed at meteorological stations and those derived from the AMSR-E from 2003 to 2007.

The Cryosphere Discuss., doi:10.5194/tc-2016-262, 2016
Manuscript under review for journal The Cryosphere
Published: 19 December 2016

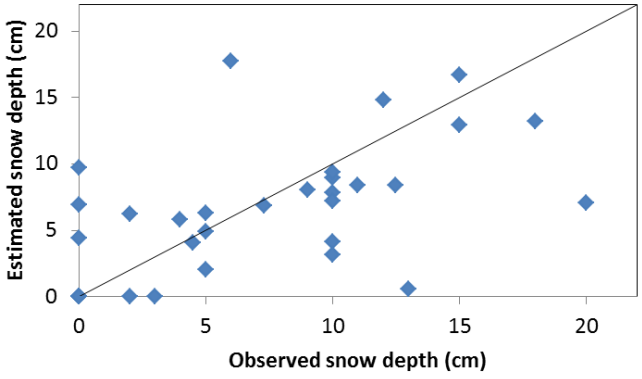

(a)

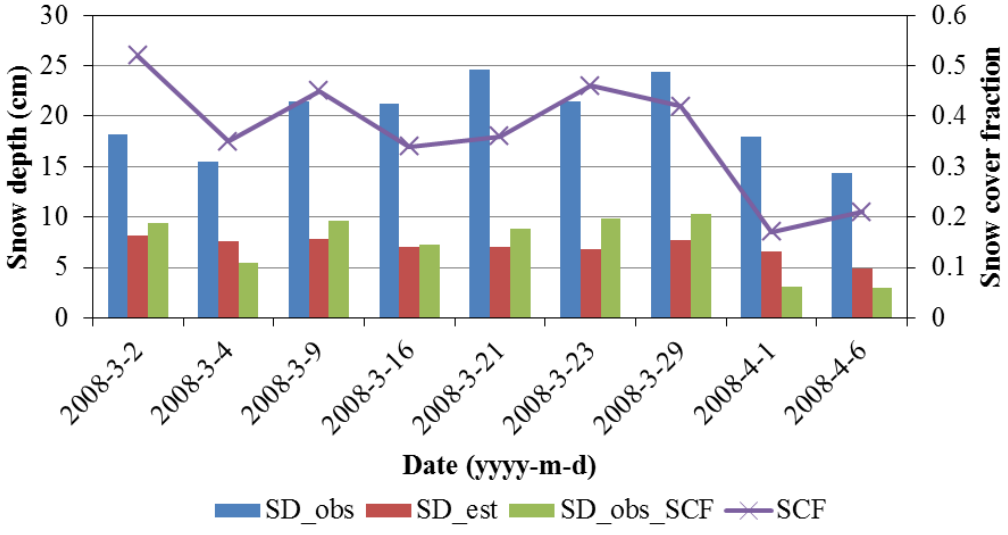

(b)

Fig.6. Comparison between measured snow depth and estimated snow depth from AMSR-E/AMSR2, (a) for March, 2014 along the observation route, (b) for March, 2008 in the Binggou watershed: bar graph of observed snow depth, area-weighted observed snow depth, and estimated snow depth from AMSR-E, and line graph of snow cover fractions on different days.

The Cryosphere Discuss., doi:10.5194/tc-2016-262, 2016
Manuscript under review for journal The Cryosphere
Published: 19 December 2016

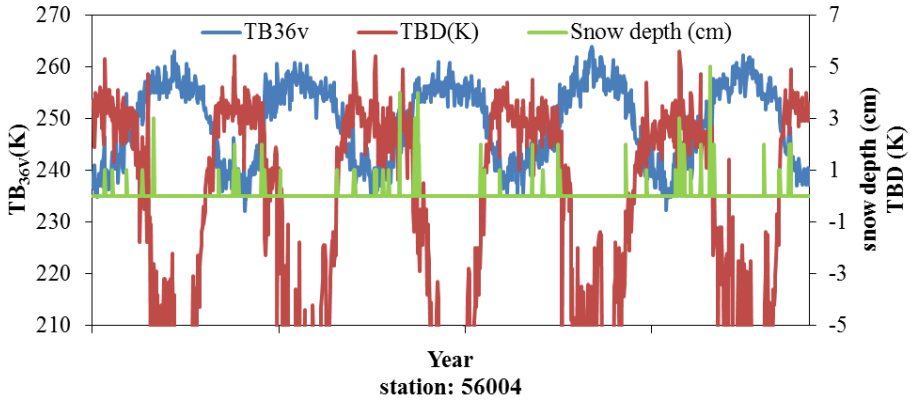

Fig. 7. Temporal variation of brightness temperature at 36 GHz for vertical polarization (TB_{36V}), TBD, and snow depth observed at Tuotuohe station (Id:56004).

The Cryosphere Discuss., doi:10.5194/tc-2016-262, 2016
Manuscript under review for journal The Cryosphere
Published: 19 December 2016

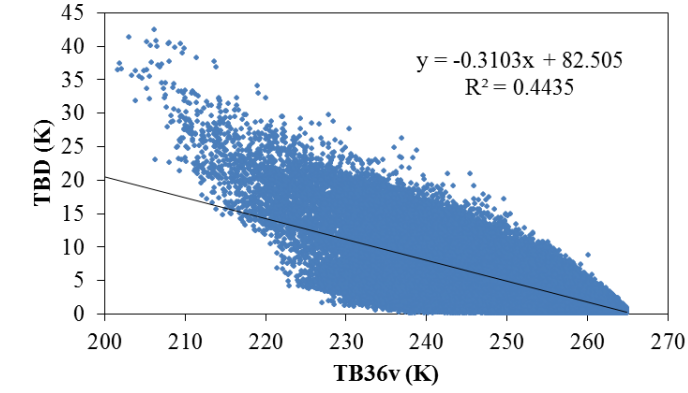

(a)

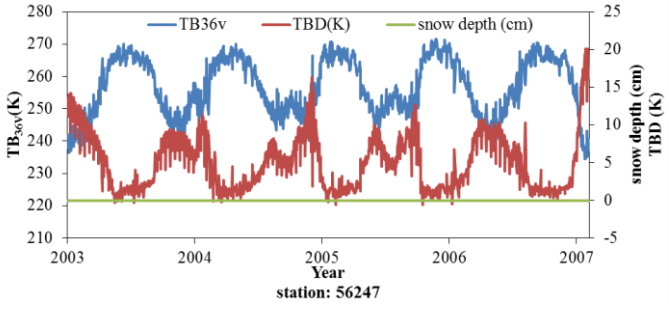

(b)

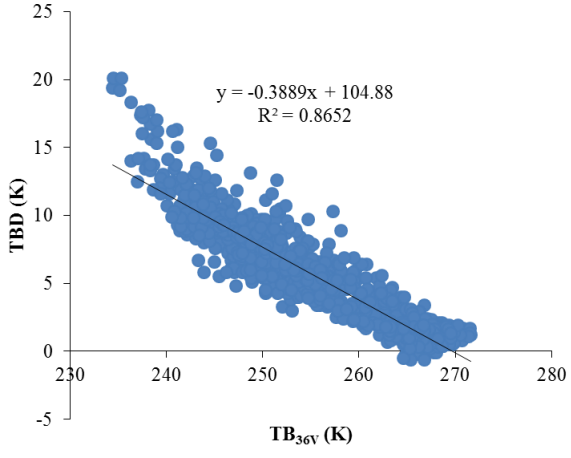

(c)

Fig. 8. Relationship between TBD and TB_{36V} at all stations (a) and Batang station (Id: 56247) (c), and the temporal variation of TB_{36V}, TBD, and snow depth observed at Batang station (b).

The Cryosphere Discuss., doi:10.5194/tc-2016-262, 2016
Manuscript under review for journal The Cryosphere
Published: 19 December 2016

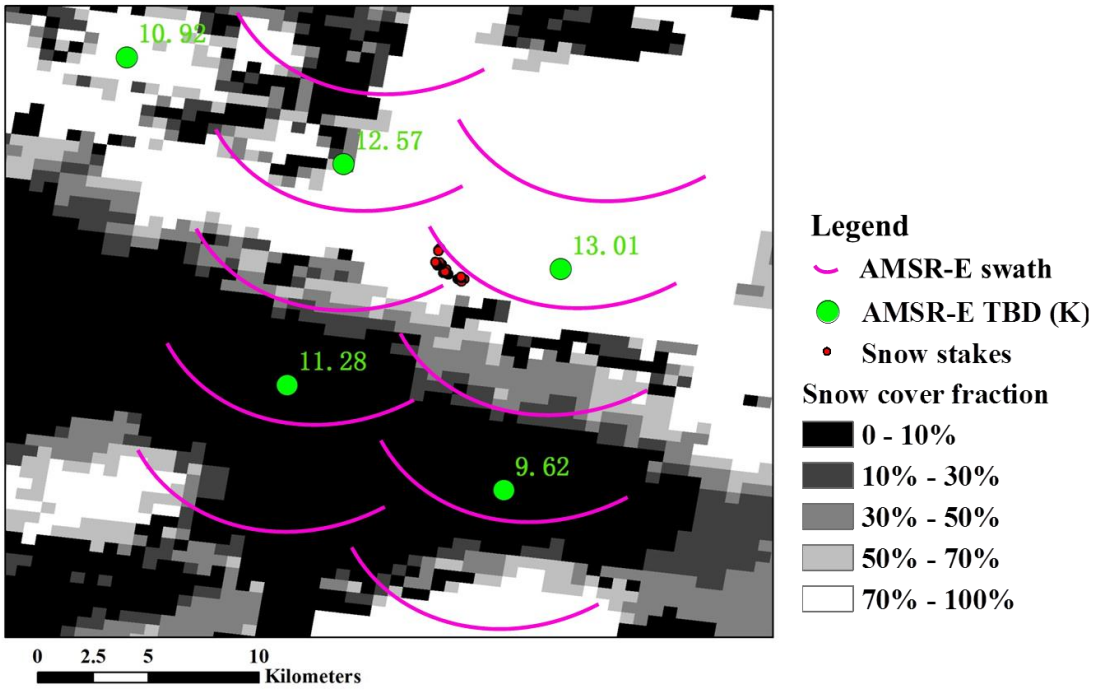

Fig. 9. Distribution of snow cover fraction derived from MODIS products in the Binggou watershed, locations of snow stakes set during the Binggou watershed experiment, and the brightness temperature difference between the 18 GHz and 36 GHz from AMSR-E.